Spin Seebeck Effect in insulating $SrFeO_{3-\delta}$ Films

Deshun Hong, Changjiang Liu, John Pearson, Axel Hoffmann, Dillon D. Fong and Anand Bhattacharya*

Materials Science Division, Argonne National Laboratory, Argonne, Illinois 60439, USA

*Email: anand@anl.gov

Abstract: In $SrFeO_{3-\delta}$, non-collinear antiferromagnetic spin textures have led to the observation of the topological Hall effect, and may give rise to novel magnetic excitations. Here, we measured the spin Seebeck effect in epitaxial, oxygen reduced $SrFeO_{3-\delta}$ films, which are non-ferromagnetic and insulating at low temperatures. We detected a spin Seebeck signal below 300 K and the signal is enhanced below ~ 100 K, near the ordering temperature of incommensurate antiferromagnetism found in bulk single crystals of $SrFeO_{3-\delta}$. The spin Seebeck signal increases in magnitude and develops a nonlinear dependence on magnetic field at lower temperatures. Control experiments were used to verify that the measured signal arises from a spin current and to rule out magnetic proximity effects. Our work shows a detectable spin Seebeck signal in non-ferromagnetic insulator $SrFeO_{3-\delta}$.

The spin Seebeck effect (SSE) is an effective way of generating pure spin currents driven by thermal gradients, and has been widely used in spintronics [1]. In general, a spin current can be carried by both mobile charges as well as magnons. Due to the latter, pure spin currents can be generated by localized spins in insulators. These spin currents can be detected via the inverse spin Hall effect in an adjacent detector layer (typically Pt or W). The SSE was first reported in the ferromagnetic metal $Ni_{81}Fe_{19}$ although the interpretation of the results is questionable [2] and soon after in the insulating ferrimagnet $LaY_2Fe_5O_{12}$ [3]. The curvature of a spin Seebeck signal as a function of magnetic field depends upon the nature of magnetic correlations in the material. In addition to ferromagnetic materials, spin Seebeck signals have also been detected in

ferrimagnetic [3-7], antiferromagnetic (AF) [8-11] and even correlated paramagnetic [12, 13] materials with distinctive signatures in the dependence of spin current on magnetic field and temperature. Recent work has shown that the SSE can be a useful tool for detecting short-range magnetic correlations in the geometrically frustrated paramagnet $Gd_3Ga_5O_{12}$ [14], and for probing unconventional magnetic excitations in the spin-chain compound Sr_2CuO_3 [15].

$SrFeO_3$ (SFO) is cubic perovskite with Fe ions in the center of oxygen octahedra [16, 17]. In a simplified picture, the electronic configuration of Fe^{4+} in SFO is $3d^4$ $(t_{2g}^3 e_g^1)$, similar to Mn^{3+} in $LaMnO_3$ (LMO). However, both the electronic and magnetic properties of SFO are very different from LMO: the latter is an *A*-type, orbital-ordered AF insulator below a Neel temperature $T_N \sim 140$ K [18, 19] with a strong Jahn - Teller distortion [20]. These differences are related to the negative charge transfer energy in SFO, which leads to a spontaneous transfer of electrons in O $2p$ orbitals to the Fe e_g orbitals [21]. Thus, instead of Fe^{4+} we have an electronic configuration of $Fe^{3+}L$ $(t_{2g}^3 e_g^2 2p^5)$ in SFO, where *L* stands for a ligand hole in O $2p$ orbital and a nominally half-filled $3d^5$ shell. Therefore, SFO is cubic without any Jahn - Teller distortion [22, 23]; furthermore, SFO shows metallic behavior over the entire temperature range with an AF transition at $T_N \sim 134$ K. This AF structure is helimagnetic with a propagation vector along [111], with a spin helix periodicity of ~18 Å [24]. Presumably arising from this textured magnetic structure, a topological Hall effect has been measured in $SrFeO_3$ at fields above 5 T [24, 25]. More recently, two types of multiple helimagnetic wavevector topological spin structures were identified in $SrFeO_3$ that appear in the absence of external fields [26].

However, due to the high valence the Fe^{4+} ion, $SrFeO_3$ is unstable and tends to reduce easily in air (losing oxygen), analogous to $SrCoO_3$ [27]. Until now, SFO has been mostly studied in bulk form, requiring post-growth annealing in high pressure or activated oxygen [16, 24], and it has been challenging to obtain stoichiometrically high quality epitaxial films by conventional techniques. Recently, using ozone-assisted molecular beam epitaxy, we have grown metallic $SrFeO_3$ films without the need for

post-growth annealing [28]. The electronic transport properties in these $SrFeO_3$ films were very close to those of the best bulk $SrFeO_3$ single crystals, indicating the high crystalline quality and stoichiometry of these films. However, while $SrFeO_3$ is AF below T_N, we were unable to measure this transition in our films using SQUID (superconducting quantum interference device) magnetometry.

In this letter, we use the longitudinal SSE to detect spin correlations in insulating, oxygen reduced $SrFeO_{3-\delta}$ films. Spin currents were generated by thermal excitation and were detected via the inverse spin Hall effect (ISHE) in a Pt or W detector layer [see Fig. 2 (a)]. Large SSE signals were measured at low temperatures and show an evolution in the magnetic field dependence. By analyzing the nonlinearity of magnetic field dependence, a transition may take place at ~ 100 K which may be related to known magnetic transitions in reduced $SrFeO_{3-\delta}$ [29].

High quality epitaxial SFO (1:1:3) films were grown on (001)-oriented $(LaAlO_3)_{0.3}(Sr_2TaAlO_6)_{0.7}$ (LSAT) single crystal substrates by ozone assisted molecular beam epitaxy. Layer-by-layer growth was realized by shuttering effusion cells sequentially, and a RHEED (reflection high energy diffraction) system was used to monitor the surface structure during growth. Detailed growth parameters can be found in [28]. For the results reported here, we grew SFO films of 60 unit cells thickness, where the as-grown films show the same behavior as bulk SFO single crystals. Fig. 1 (a) shows that the RHEED intensity oscillates periodically during growth until the last monolayer. To exclude magnetic proximity effects in our SSE measurement, films with two extra SrO 'exchange blocking' layers [the red line in Fig. 1 (a)] were also grown as control samples. According to our X-ray diffraction data [Fig. 1S (a)], the SFO (002) peak is at a slightly higher angle than LSAT (002) peak, with a calculated c-axis lattice parameter of around 3.83 Å. The films also have the anticipated thickness of 60 u.c. or 23.0 nm according to our x-ray reflectivity measurements (not shown here). The film has a roughness of ~ 0.1 nm as measured by atomic force microscopy (AFM) [Fig. 1 (b)]. Four-terminal resistivity versus temperature (T) measurements of our as-grown film is shown in Fig. 1S (b). The behavior is similar to the R vs T in the best bulk single

crystals of SFO (1:1:3) and two transitions can be clearly seen which are attributed to the occurrence of different magnetic transitions [24].

As mentioned earlier, using conventional magnetometry, we were unable to detect magnetism in our thin films. However, given the sensitivity of the SSE to a variety of magnetic correlations, we patterned SSE devices to probe magnetic excitations in SFO. Photo-lithography, argon ion-milling, and electron beam evaporation were used to fabricate the devices. To protect the film's stoichiometry, liquid N_2 was used to cool the sample during the ion-milling step. A schematic of a patterned device is shown in Fig. 2 (a). The SFO film was first patterned into a $10 \times 800\ \mu m^2$ stripe; then a layer of Pt (5 nm) was sputtered and patterned onto the bar structure. On top of this, MgO (150 nm) and Au (50 nm) were evaporated sequentially as electrical insulator and heater respectively. As we have shown in previous work, SFO films are highly sensitive to moisture and readily reduced in air [27]. Thus, despite our efforts to preserve oxygen stoichiometry, the films became insulating after patterning, and the two-terminal resistance of our devices was > 60 MΩ at 300 K. Therefore, the SFO films in our SSE devices are reduced to $SrFeO_{3-\delta}$. As can be seen in Fig. 2S, SFO film's Bragg peak moves a lot before and after patterning, corresponding to the d spacing change from 3.83 to 3.95, consistent with the fully insulative behavior. However, a benefit of having insulating behavior in the $SrFeO_{3-\delta}$ films over the whole temperature range is that the SSE signals from our samples are not affected by the Nernst effect in SFO.

In our measurements, a 3 Hz sinusoidal 1 V_{pp} signal was applied across the heater (~ 60 Ω) resulting in a heat flux of ~ 0.20 W/mm^2, generating an out-of-plane thermal gradient. Applying an in-plane magnetic field perpendicular to the SFO stripe, the voltage across the Pt detector was measured at the second harmonic using a lock-in technique. As can be seen in Fig. 2 (b), there is almost no signal when the magnetic field is zero. By ramping the magnetic field between -9 T and 9 T, a voltage can be measured. For the longitudinal SSE set up with the on-chip heater, the measurement can be performed at temperatures as low as 2 K. The field-dependent voltage measurement shows nonlinear behavior, as can be seen in Fig. 2 (c). This nonlinearity

with field is presumably related to the excitation of magnons in SFO and the change in their chemical potential in an applied magnetic field, as has been observed in SSE measurements on ferromagnets [30], antiferromagnets [11] and correlated paramagnets [12].

We checked the magnetic origin of the measured signal by measuring the angular dependence of the SSE voltage with a constant 9 T field at 10 K. A sinusoidal behavior was observed, as shown in Fig. 2 (d). To protect the bonded wires from rupture by Lorentz forces, we decreased the thermal power to ~ 0.05 W/mm^2 for measurements in high magnetic fields, as shown in Fig. 2 (c) and Fig. 2 (d). For fields applied in-plane and perpendicular to the wire, at high temperatures [Fig. 2 (b)], the measured voltage is relatively small (0.2 μV) and grows monotonically upon lowering the temperature to as much as to 1.8 μV at 2 K and 9 T, which is comparable with YIG for a similar heat flux. Notably, at higher temperatures, the magnitude of the SSE signal decreases relatively slowly and can still be easily resolved at 300 K. In $SrFeO_{3-\delta}$, for $0 < \delta < 0.23$, all magnetic order is strongly suppressed for T > 150 K [28]. For $\delta = 0.5$, AF order develops at T = 673 K. Our attempts thus far to resolve AF ordering in our reduced SFO films at 300 K using x-ray linear dichroism measurements at the Fe *L*-edge have failed. We thus presume that the high temperature SSE signal is generated from spin excitations in a nominally paramagnetic SFO film.

To verify that the signal we measured is from the SSE, we measured control samples, as shown in Fig. 3 (a). To rule out the proximity effect, two extra SrO capping layers were grown on the FeO_2-terminated 60 uc SFO, which was then patterned into devices using the same procedures. As is shown in the red curve in Fig. 3 (a), the angular dependence of the SSE from these samples has the same behavior as the SFO sample without the two SrO capping layers. The smaller amplitude is reasonable considering the attenuation of the spin current by the two SrO layers. Furthermore, by replacing Pt with W, the sign of measured voltage is reversed, which is expected because of the opposite sign of the spin Hall angle between Pt and W [31]. Besides the out-of-plane thermal gradient, there can be an in-plane component of the thermal gradient arising

from possible mis-alignment between the Au heater wire and SFO wire or the inhomogeneity of thermal diffusion at the edges of the heater wire. Thus, a Nernst signal may appear in the detector layer along with the SSE signal from the SFO. The shape of the angular dependence shifts to slightly lower angle for the device with a W detector layer [black curve in Fig. 3 (a)], which mainly comes from the Nernst effect (NE) in W. Fig. 3 (b) and Fig. 3 (c) show the temperature dependence in 60 SFO + 2 SrO film with Pt and W as spin detector, respectively. Although the amplitude of the SSE signal is smaller, the behavior in Pt devices is the same as in Fig. 2 (b). In the W devices, however, there is a crossing between +9 T and -9 T, as shown in Fig. 3 (c). The sign of voltage is the same as that in Pt devices at high temperatures while it is opposite at low temperatures. This is because the signal we measure in the W and Pt devices are a combination of SSE from SFO and the Nernst effect in the spin detector (Pt/W) layer. Both Pt and W have the same sign of the Nernst effect, while they produce SSE signals with opposite signs due to the difference of sign in their spin Hall angles. As temperature decreases, the SSE response increases and eventually overcomes the Nernst signal in the W device. In Fig. 3S, we measured signal from W with SFO and W without SFO devices, directly showing the amplitudes of SSE and NE signals, which further indicates a spin Seebeck signal from SFO even at room temperature.

As mentioned earlier, $SrFeO_{3-\delta}$ shows a variety of magnetic/electronic phases. $SrFeO_3$ ($\delta = 0$) remains metallic down to the lowest temperatures, with a paramagnetic to helicoidal AF transition at ~ 134 K. However, our films are reduced to $SrFeO_{3-\delta}$ and become insulating after patterning, with an unknown δ value. In bulk samples, for $0 \leq \delta \leq 0.19$, the $SrFeO_{3-\delta}$ magnetic susceptibility, transport and Mossbauer effect measurements show evidence for magnetic (AF) and charge-ordering at $T < 75$ K [32]. Using neutron scattering from single crystal $SrFeO_{3-\delta}$ samples with similar values of δ, an incommensurate magnetic order (with a wavevector close to that for samples with $\delta = 0$) was found to set in below ~ 130 K, while commensurate AF phases developed for $T < 75$ K [28]. For more heavily reduced $SrFeO_{3-\delta}$ ($\delta = 0.5$, Fe^{3+}), neutron scattering and magnetic susceptibility measurements show that an AF state is obtained at 673 K,

well above room temperature [33,34].

We relate these prior findings regarding the magnetic structure of $SrFeO_{3-\delta}$ to our measurements of the SSE as a function of magnetic field and temperature. As shown in Fig. 4 (a), we compared the field dependence of SSE signal at cryogenic temperatures. A very non-linear curvature can be seen at 10 K. As the temperature going up, this nonlinearity becomes weaker and can hardly be resolved at 100 K and 120 K, which can be more clearly seen in the normalized SSE signal in Fig. 4 (b). As we mentioned previously, this nonlinearity transition temperature is in the vicinity of where incommensurate magnetic order has been observed in $SrFeO_{3-\delta}$ for $0 \leq \delta \leq 0.23$. Thus, the increase in the SSE signal below 100 K may be related to the onset of incommensurate AF order in $SrFeO_{3-\delta}$.

In summary, we have performed SSE measurements on epitaxial $SrFeO_{3-\delta}$ films, and observed a spin current generation. The film is oxygen reduced and becomes insulating after patterning, which eliminates the contribution of the Nernst signal from SFO in the longitudinal SSE measurement. Control experiments were used to verify the measured signal is due to SSE. We further observed that the magnetic field dependence of the SSE signal starts to show a nonlinearity at temperatures below about 100 K, close to the incommensurate magnetic ordering temperature in $SrFeO_{3-\delta}$. Further theoretical analysis is required in order to understand the possible connection between our SSE measurement and magnetic structures in $SrFeO_{3-\delta}$.

Supplementary Material

See supplementary materials for the XRD results of SFO before and after patterning. Temperature dependence of SSE signals on control devices are also shown taking thermal conductivity into consideration.

Acknowledgement

Work at Argonne National Laboratory, including the use of the Center for Nanoscale Materials, was supported by the U.S. Department of Energy, Basic Energy Sciences.

All work was supported by the U.S. Department of Energy, Office of Science, Materials Science and Engineering Division. Lithography was performed at the Center for Nanoscale Materials, which is supported by DOE-BES under Contract No. DE-AC02-06CH11357. The authors acknowledge Brandon Fisher, Terence Michael Bretz-Sullivan and Frederike Wrobel for experimental help and fruitful discussions.

Reference

[1] G. E. W. Bauer, E. Saitoh, and B. J. van Wees, *Nat. Mater.* **11**. 391 (2012).

[2] K. Uchida, S. Takahashi, K. Harii, J. Ieda, W. Koshibae, K. Ando, S. Maekawa & E. Saitoh, *Nature* **455**, 779 (2008).

[3] K. Uchida, J. Xiao, H. Adachi, J. Ohe, S. Takahashi, J. Ieda, T. Ota, Y. Kajiwara, H. Umezawa, H. Kawai, G. E. Bauer, S. Maekawa and E. Saitoh, *Nat. Mater.* **9**, 894–897 (2010).

[4] K. Uchida, H. Adachi, T. Ota, H. Nakayama, S. Maekawa & E. Saitoh, *Appl. Phys. Lett.* **97**, 172505 (2010).

[5] D. Qu, S. Y. Huang, J. Hu, R. Wu & C. L. Chien, *Phys. Rev. Lett.* **110**, 067206 (2013).

[6] A. Kehlberger, U. Ritzmann, D. Hinzke, E.-J. Guo, J. Cramer, G. Jakob, M. C. Onbasli, D. H. Kim, C. A. Ross, M. B. Jungfleisch, B. Hillebrands, U. Nowak & M. Klaui, *Phys. Rev. Lett.* **115**, 096602 (2015).

[7] P. Li, D. Ellsworh, H. Chang, P. Janatha, D. Richardson, F. Shah, P. Phillips, T. Vijayasarathy, and M. Wu, *Appl. Phys. Lett*. 105, 242412 (2014).

[8] Y. Ohnuma, H. Adachi, E. Saitoh & S. Maekawa, *Phys. Rev. B* **87**, 014423 (2013).

[9] S.Seki, T. Ideue, M. Kubota, Y. Kozuka, R. Takagi, M. Nakamura, Y. Kaneko, M. Kawasaki, and Y. Tokura, *Phys. Rev. Lett.* **115**, 266601 (2015).

[10] J. Holanda, D. S. Maior, O. A. Santos, L. H. Vilela-Leao, J. B. S. Mendes, A. Azevedo, R. L. Rodriguez-Suarez, and S. M. Rezende, *Appl. Phys. Lett.* **111**, 172405 (2017).

[11] S. M. Wu, W. Zhang, A. KC, P. Borisov, J. E. Pearson, J. S. Jiang, D. Lederman, A. Hoffmann & A. Bhattacharya, *Phys. Rev. Lett.* **116**, 097204 (2016).

[12] S. M. Wu, J. E. Pearson & A. Bhattacharya, *Phys. Rev. Lett.* **114**, 186602 (2015).

[13] A. Aqeel, N. Vlietstra, J. A. Heuver, G. E. W. Bauer, B. Noheda, B. J. van Wees & T. T. M. Palstra, *Phys. Rev. B* **92**, 224410 (2015).

[14] C. Liu, S. M. Wu, J. E. Pearson, J. S. Jiang, N. d'Ambrumenil & Anand Bhattacharya, *Phys. Rev. B* **98**, 060415 (R) (2018).

[15] D. Hirobe, M. Sato, T. Kawamata, Y. Shiomi, K. Uchida, R. Iguchi, Y. Koike, S. Maekawa & E. Saitoh, *Nat. Phys.* **13**, 30-34 (2017).

[16] A. Lebon, P. Adler, C. Bernhard, A. V. Boris, A. V. Pimenov, A. Maljuk, C. T. Lin, C. Ulrich & B. Keimer. *Phys. Rev. Lett.* **92**, 037202 (2004).

[17] P. Adler, A. Lebon, V. Damljanovic, C. Ulrich, C. Bernhard, A.V. Boris, A. Maljuk, C. T. Lin & B. Keimer, *Phys. Rev. B* **73**, 094451 (2006).

[18] E. O. Wollan & W. C. Koehler, *Phys. Rev.* **100**, 545 (1995).

[19] N. N. Kovaleva, A. V. Boris, C. Bernhard, A. Kulakov, A. Pimenov, A. M. Balbashov, G. Khaliullin & B. Keimer, *Phys. Rev. Lett.* **93**, 147204 (2004).

[20] J. Rodriguez – Carvajal, M. Hennion, F. Moussa, A. H. Moudden, L. Pinsard & A. Revcolevschi, *Phys. Rev. B* **57**, R3189 (1998).

[21] M. Mostovoy, *Phys. Rev. Lett.* **94**, 137205 (2005).

[22] P. K. Gallagher, J. B. McChesney & D. N. E. Buchanan, *J. Chem. Phys.* **41**, 2429 (1964).

[23] J. B. McChesney, R. C. Sherwood & J. F. Potter, *J. Chem. Phys.* **43**, 1907 (1965)

[24] S. Ishiwata, M. Tokunaga, Y. Kaneko, D. Okuyama, Y. Tokunaga, S. Wakimoto, K. Kakurai, T. Arima, Y. Taguchi & Y. Tokura, *Phys. Rev. B* **84**, 054427 (2011).

[25] S. Chakraverty, T. Matsuda, H. Wadati, J. Okamoto, Y. Yamasaki, H. Nakao, Y. Murakami, S. Ishiwata, M. Kawasaki, Y. Taguchi, Y. Tokura & H. Y. Hwang, *Phys. Rev. B* **88**, 220405 (R) (2013).

[26] S. Ishiwata, T. Nakajima, J. -H. Kim, D. S. Inosov, N. Kanazawa, J. S. White, J. L. Gavilano, R. Georgii, K. SeeMann, G. Brandl, P. Manuel, D. D. Khalyavin, S. Seki, Y. Tokunaga, M. Kinoshita, Y. W. Long, Y. Kaneko, Y. Taguchi, T. Arima, B. Keimer, and Y. Tokura, *ArXiv:* 1806.02309.

[27] H. Jeen, W. S. Choi, M. D. Biegalski, C. M. Folkman, I-C. Tung, D. D. Fong, J. W. Freeland, D. Shin, H. Ohta, M. F. Chisholm & H. N. Lee, *Nature Mater.* **12**, 1057 (2013).

[28] D. Hong, C. Liu, J. Pearson & A. Bhattacharya, *Appl. Phys. Lett.* **111**, 232408 (2017).

[29] M.Reehuis, C. Ulrich, Ch. Niedermayer, B. Ouladiaf, A. Hoser, T. Hofmann, and B. Keimer, *Phys. Rev. B* **85**, 184109 (2012).

[30] T. Kikkawa, K.-i. Uchida, S. Daimon, Z. Qiu, Y. Shiomi and E. Saitoh, *Phys. Rev. B* **92**, 064413 (2015).

[31] A. Hoffmann, *IEEE Trans. Magn.* **49**, 5172 (2013).

[32] A. Lebon, P. Adler, C. Bernhard, A. V. Boris, A. V. Pimenov, A. Maljuk, C. T. Lin, C. Ulrich & B. Keimer, *Phys. Rev. Lett.* **92**, 037201 (2004).

[33] M. Schmidt and S. J. Campbell, *J. Solid State Chem*. **156**, 292 (2001).

[34] J.-C. Grenier, N. Ea, M. Pouchard, and P. Hagenmuller, *J. Solid State Chem*. **58**, 243 (1985).

Fig. 1.

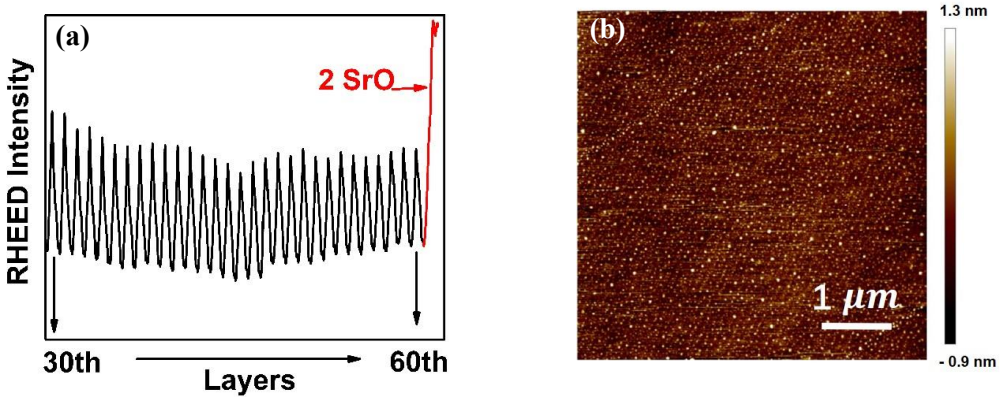

Fig. 1 (a) RHEED oscillations during growth of SFO. For clarity, oscillations from 30th to 60th u.c. are plotted. The red curve shows the RHEED intensity during SrO growth. (b) Morphology of SFO film by AFM with the scale bar ranging 1 μm.

Fig. 2.

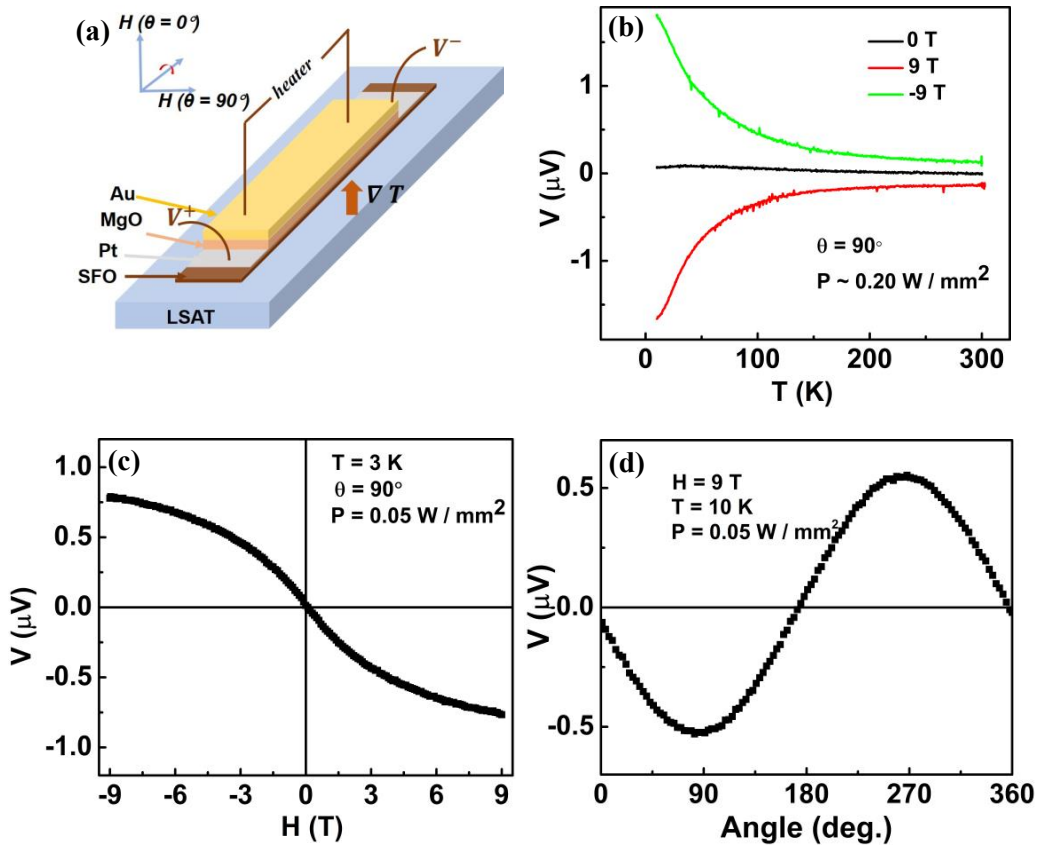

Fig. 2 (a) Schematic of patterned SSE device. (b) Temperature dependence of the spin Seebeck voltage response at 0 T, 9 T and -9 T in one SFO-Pt device with 0.2 W/mm^2 thermal flux. (c) Field-dependent voltage response with 0.05 W/mm^2 at 3 K. (d) Angular-dependent voltage responses with a constant 9 T field and 0.05 W/mm^2 thermal power at 10 K. According to our convention, H (90°) = 9 T and H (270°) = -9 T. We lowered the heater power in (c) and (d) to protect bonded wires.

Fig. 3

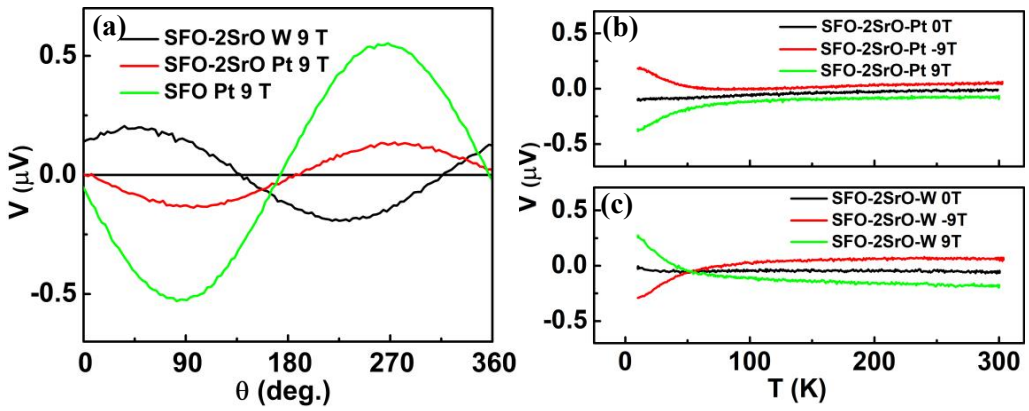

Fig. 3 (a) Angular-dependent voltage responses with a constant 9 T field at 10 K in three devices. Temperature dependence of the spin Seebeck voltage response at 0 T, 9 T and -9 T in SFO-2SrO-Pt device (b) and SFO-2SrO-W device (c). The heater power is 0.05 W/mm^2 during above measurements and $\theta = 90°$ in both (b) and (c).

Fig. 4

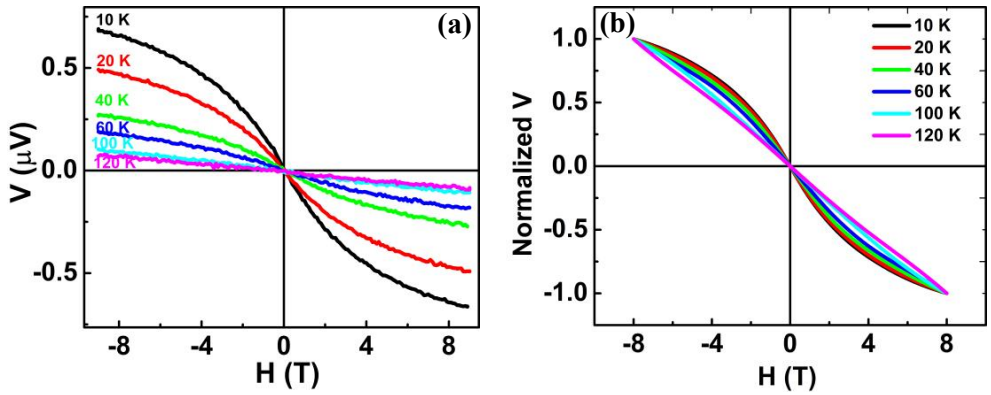

Fig. 4 (a) Field dependence of SSE signal and (b) Normalized SSE signal at various temperatures. A transition from non-linear to linear can be seen when the sample was heated above 100 K which may be related to incommensurate magnetic order in $SrFeO_{3-\delta}$.

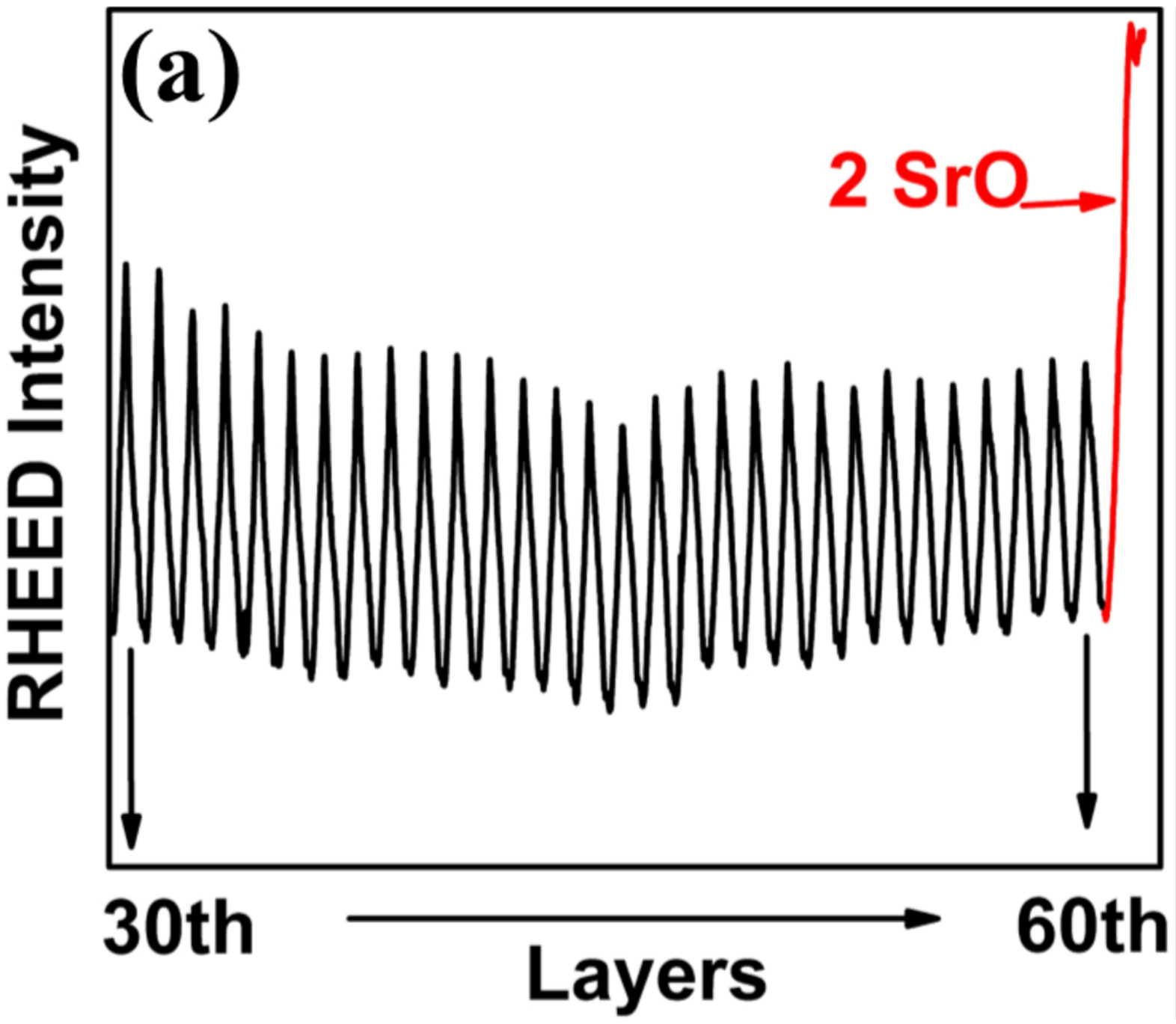
(a)
2 SrO
RHEED Intensity
30th
60th
Layers

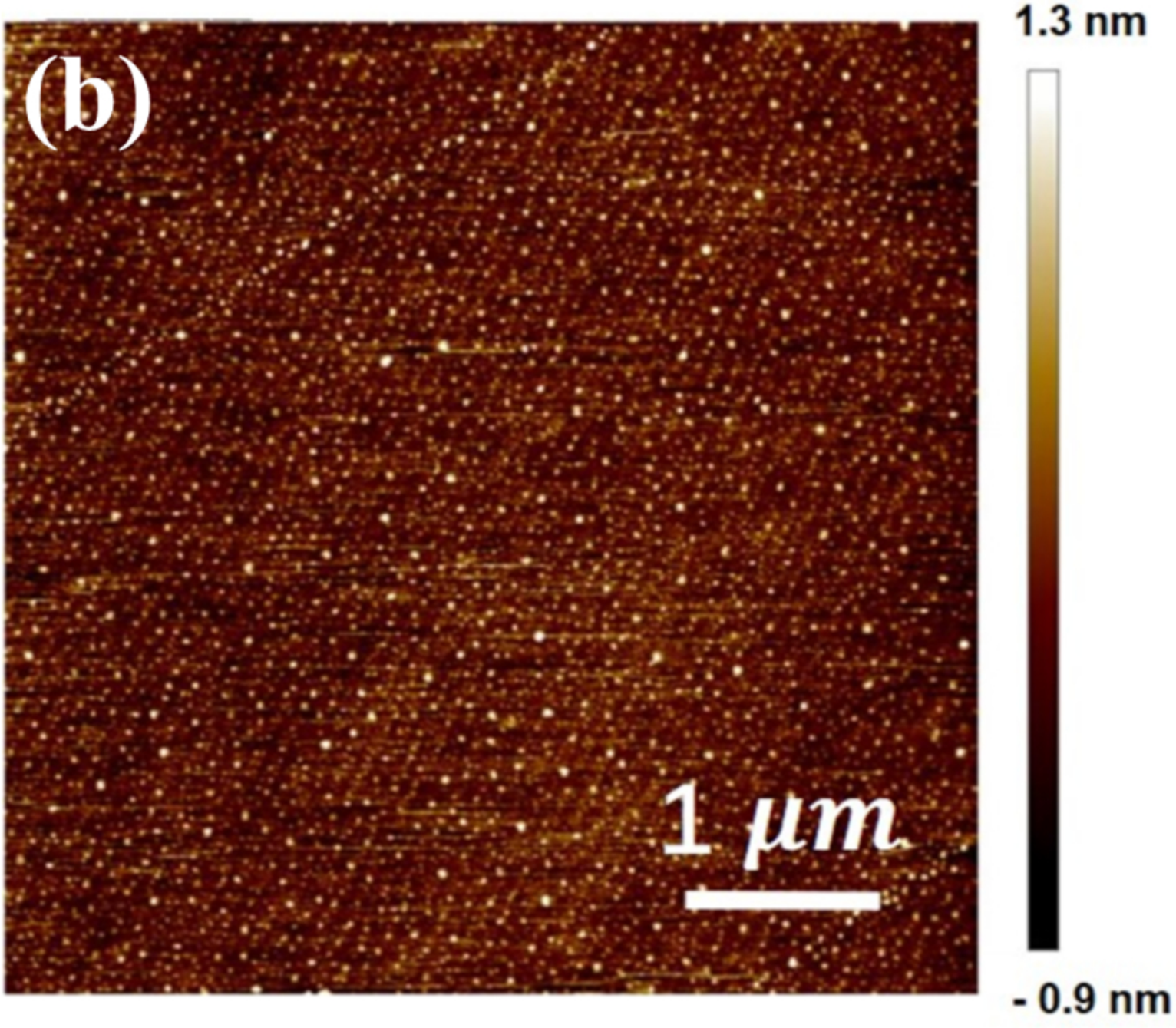
(b)
1 μm
1.3 nm
- 0.9 nm

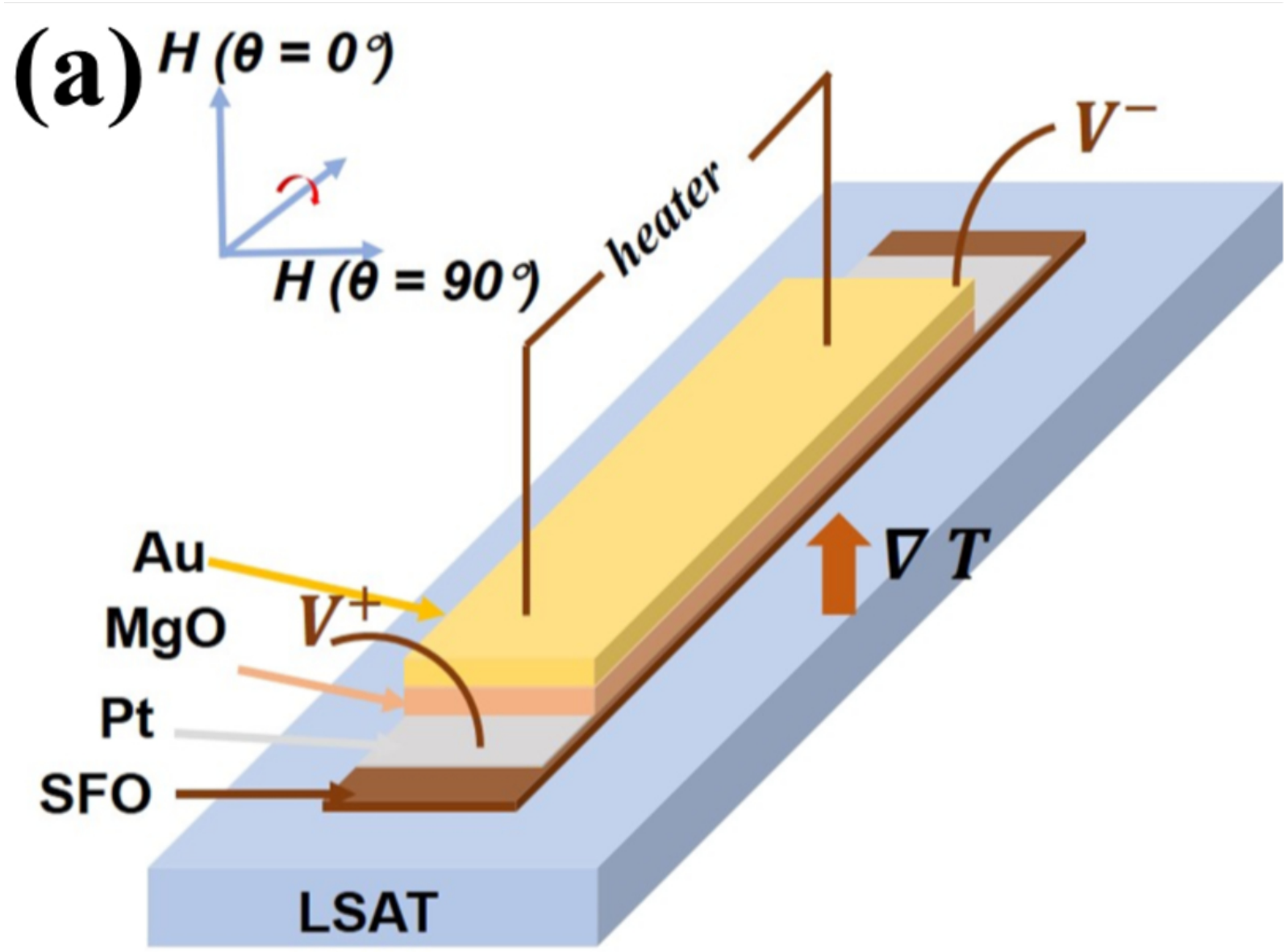
(a)
H (θ = 0°)
H (θ = 90°)
heater
V−
Au
MgO
V+
Pt
SFO
∇T
LSAT

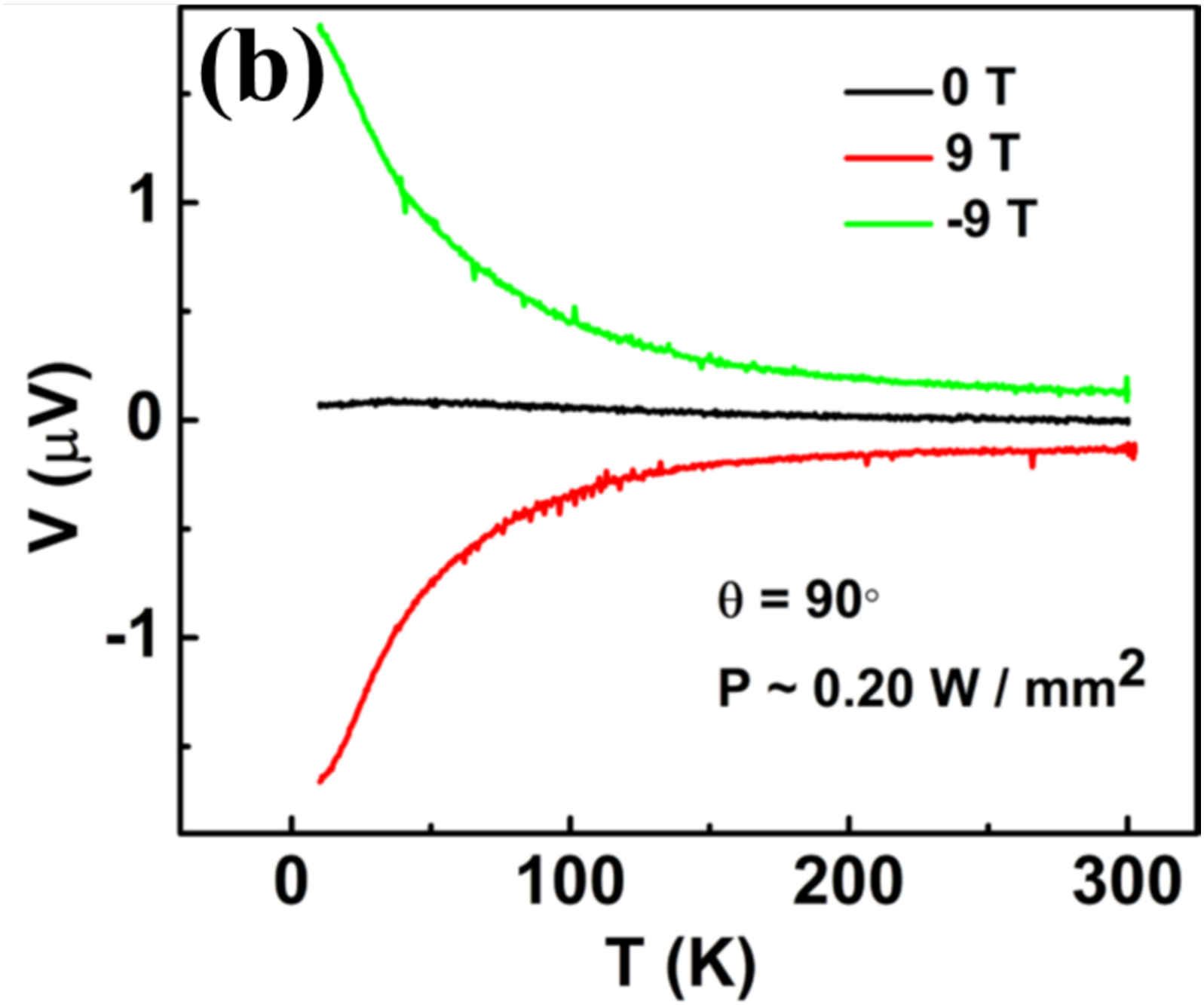
(b)
0 T
9 T
-9 T
θ = 90°
P ~ 0.20 W / mm2
V (μV)
1
0
-1
0
100
200
300
T (K)

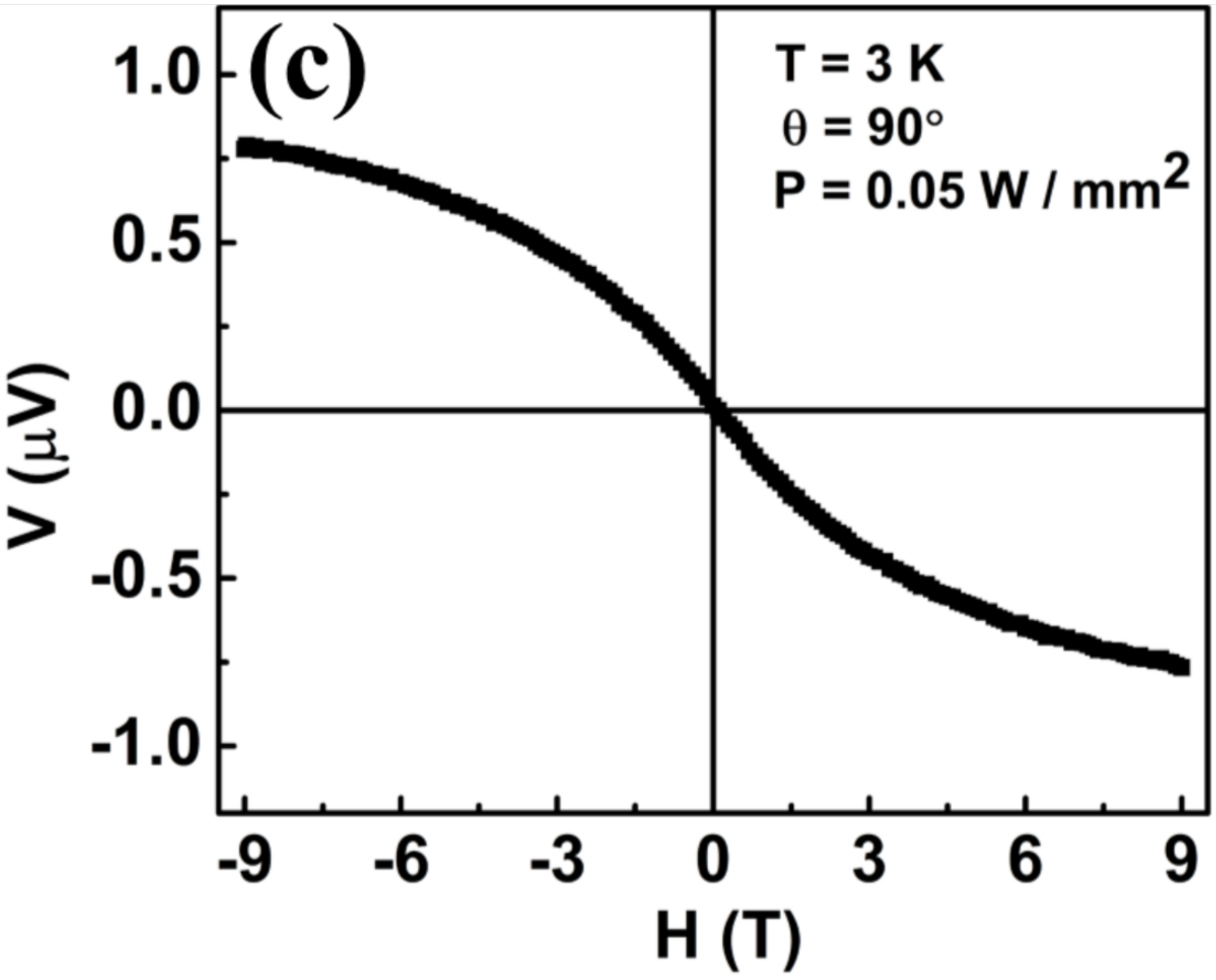
(c)
T = 3 K
θ = 90°
P = 0.05 W / mm2
1.0
0.5
0.0
-0.5
-1.0
V (μV)
-9
-6
-3
0
3
6
9
H (T)

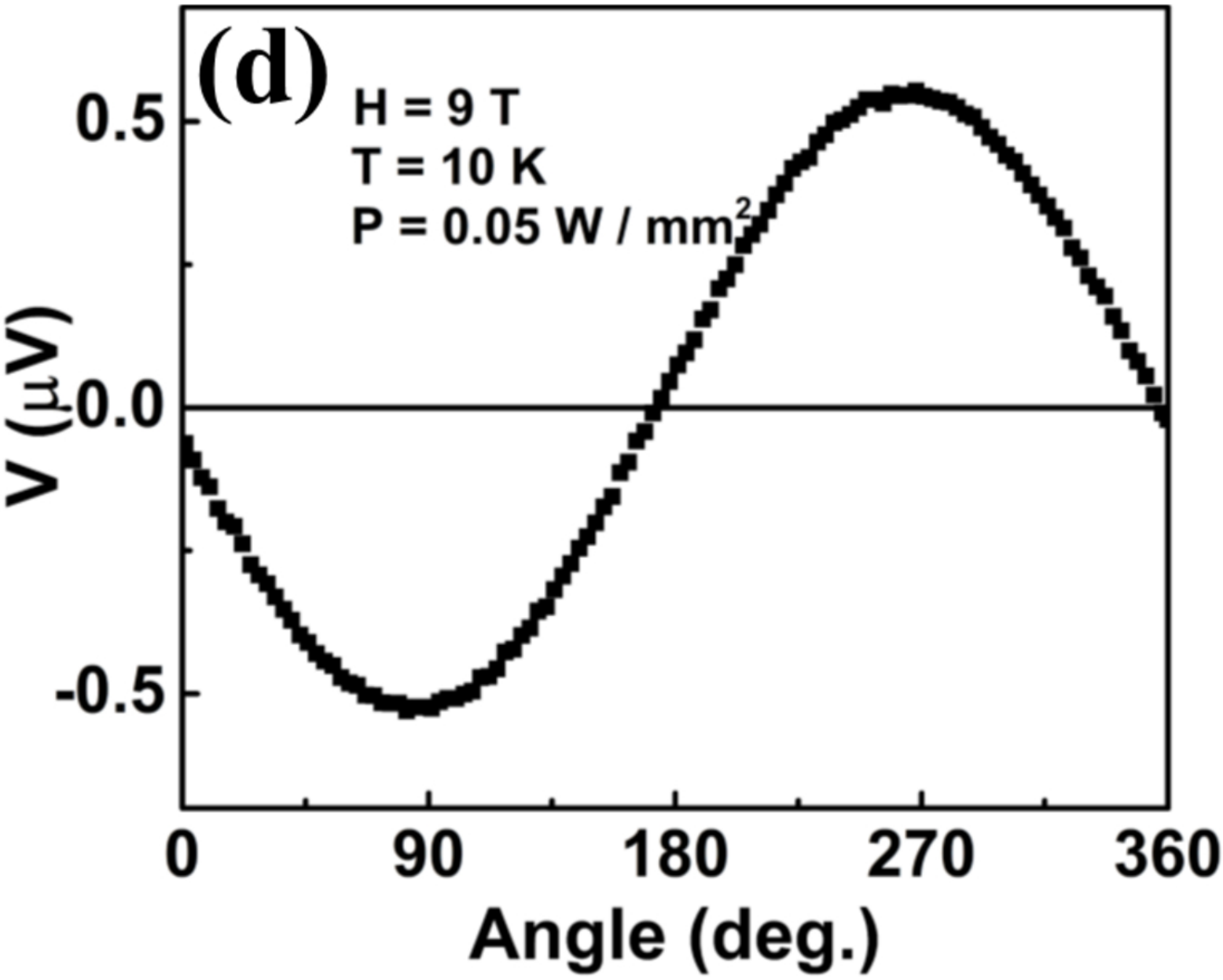
(d)
H = 9 T
T = 10 K
P = 0.05 W / mm2
0.5
0.0
-0.5
V (μV)
0
90
180
270
360
Angle (deg.)

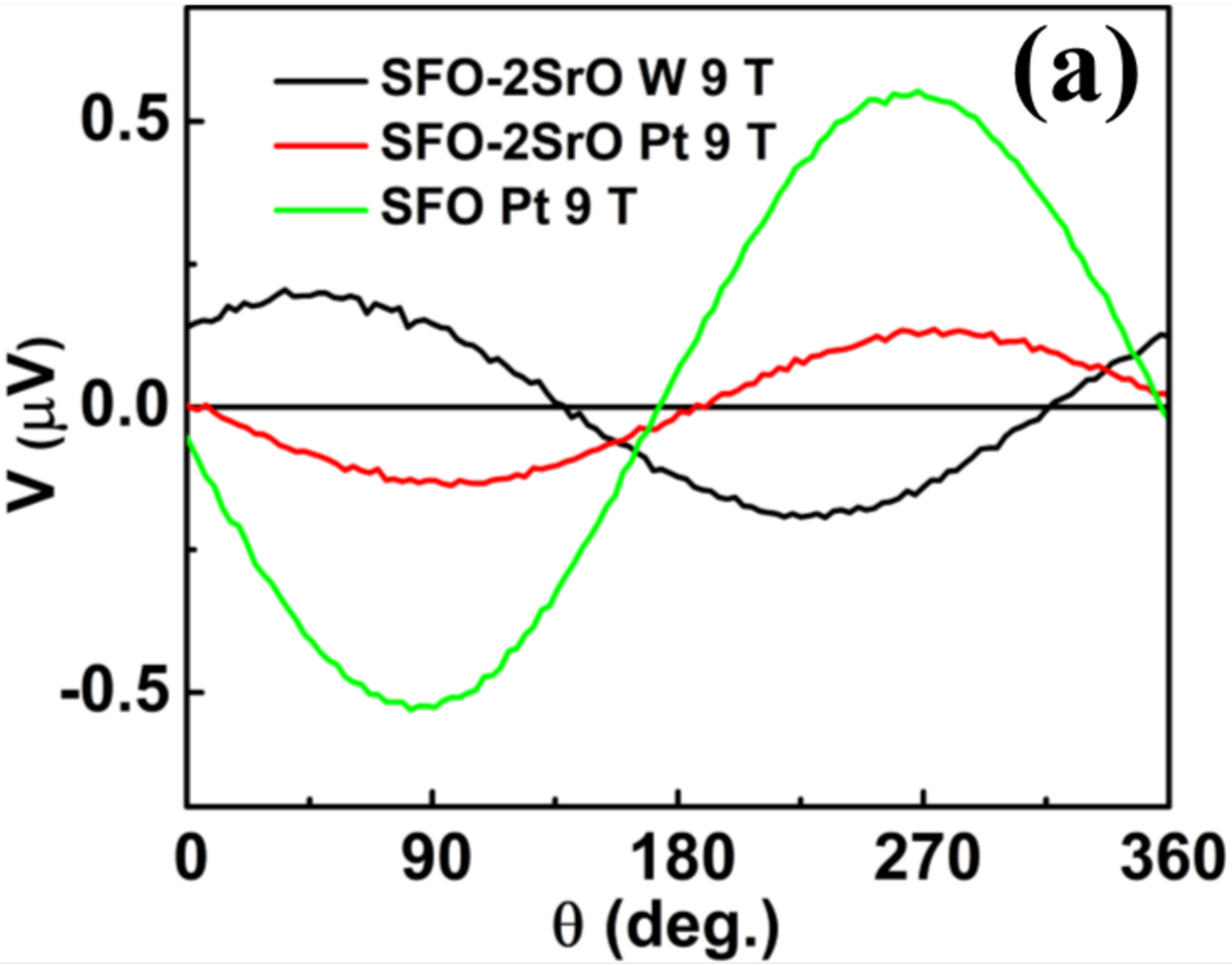
(a)
SFO-2SrO W 9 T
SFO-2SrO Pt 9 T
SFO Pt 9 T
0.5
0.0
-0.5
V (μV)
0
90
180
270
360
θ (deg.)

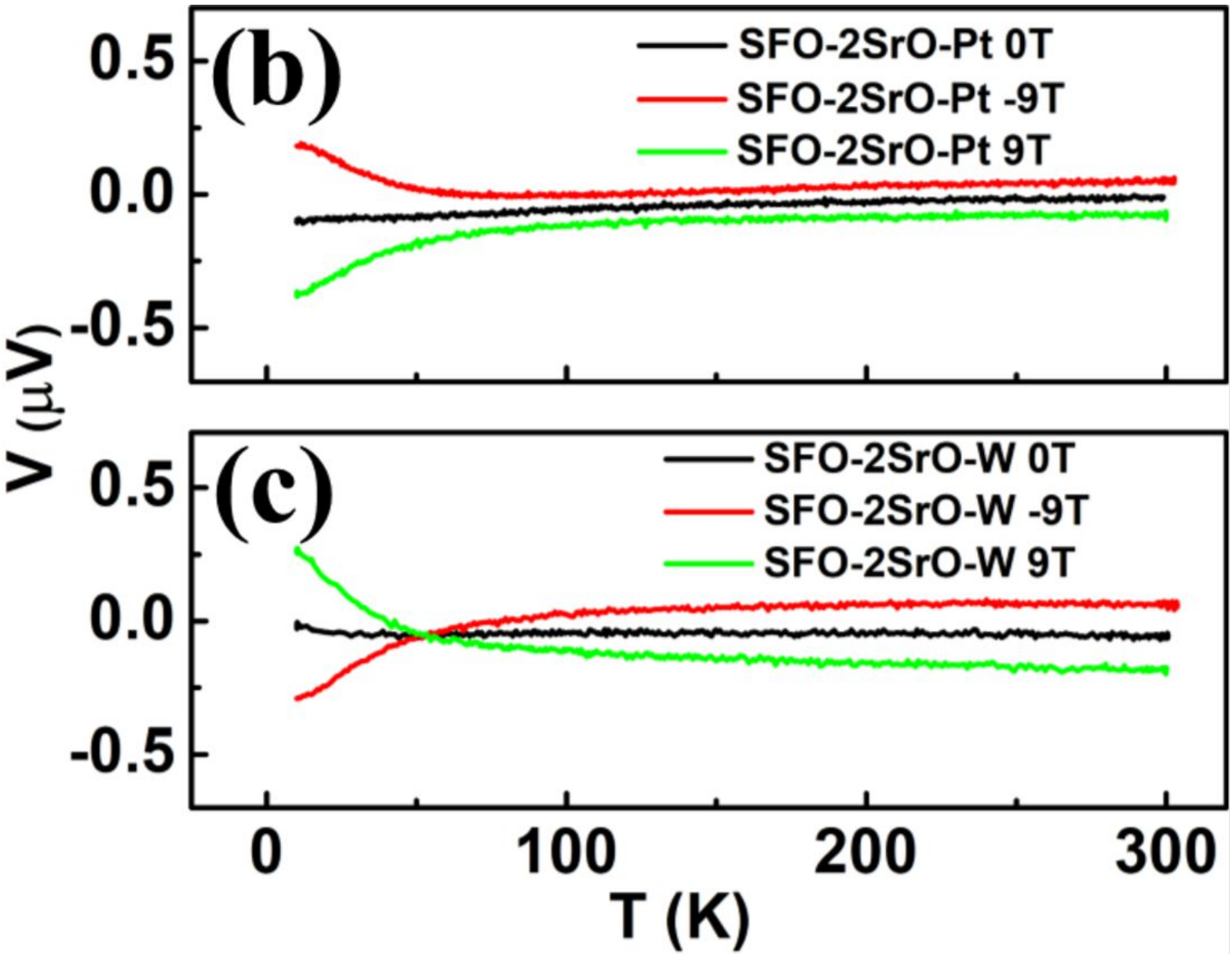
(b)
SFO-2SrO-Pt 0T
SFO-2SrO-Pt -9T
SFO-2SrO-Pt 9T
0.5
0.0
-0.5
(c)
SFO-2SrO-W 0T
SFO-2SrO-W -9T
SFO-2SrO-W 9T
V (μV)
0
100
200
300
T (K)

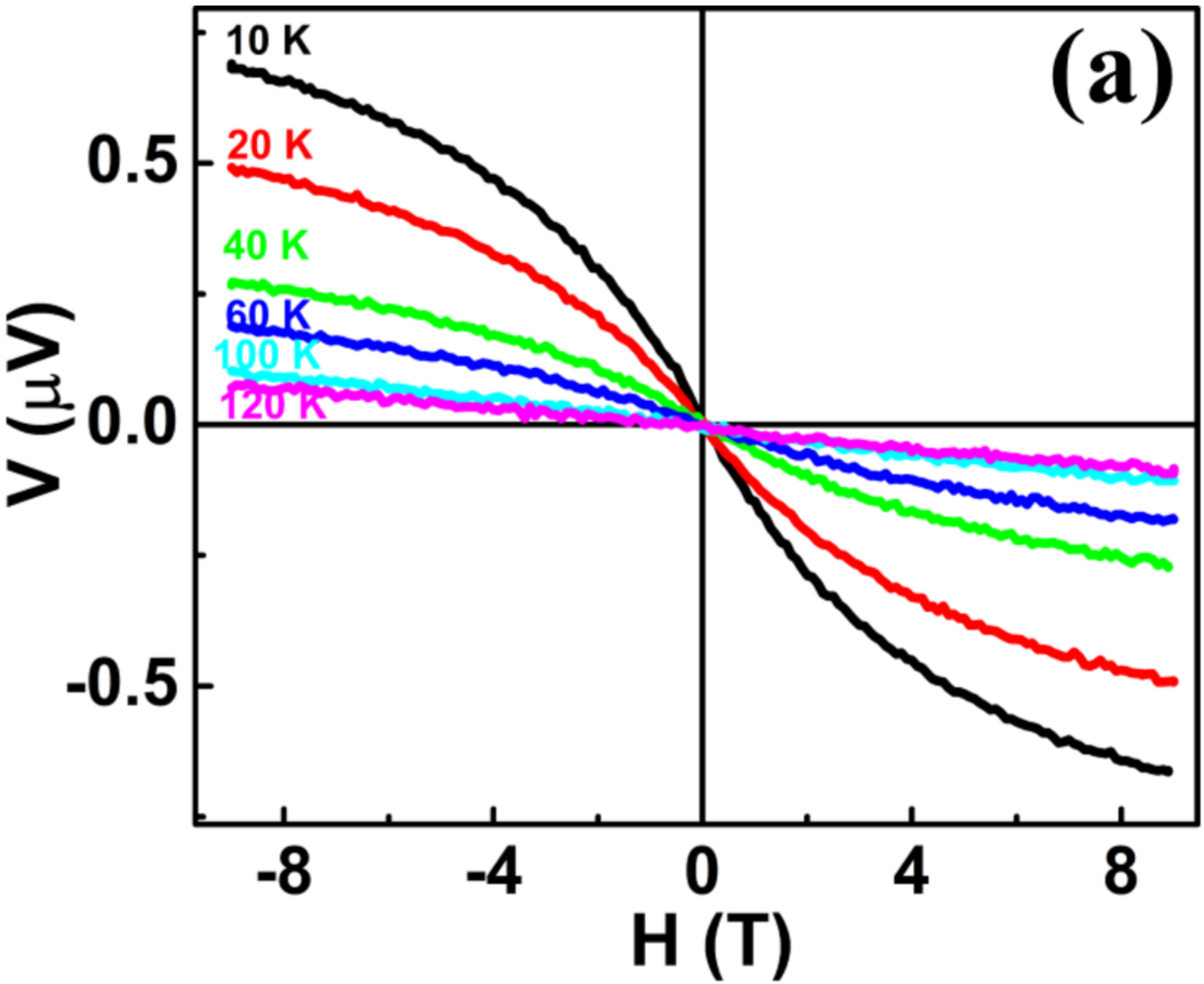
(a)
10 K
20 K
40 K
60 K
100 K
120 K
0.5
0.0
-0.5
V (μV)
-8
-4
0
4
8
H (T)

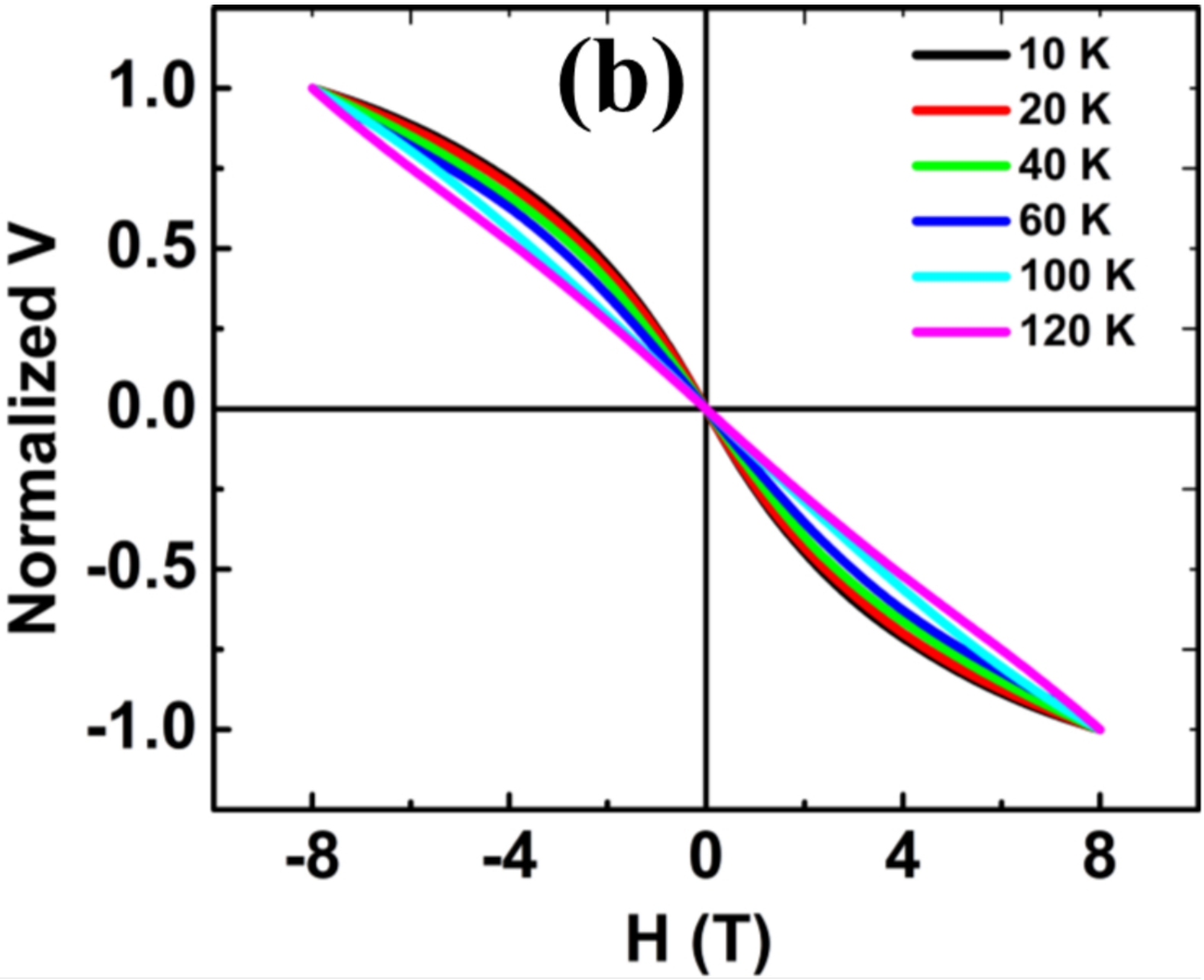
(b)
10 K
20 K
40 K
60 K
100 K
120 K
Normalized V
1.0
0.5
0.0
-0.5
-1.0
-8
-4
0
4
8
H (T)